Structure of iron niobophosphate glasses investigated by DTA, infrared and Mössbauer spectroscopy

1998 J. Phys.: Condens. Matter 10 7511

(http://iopscience.iop.org/0953-8984/10/34/005)

J. Phys.: Condens. Matter **10** (1998) 7511–7518. Printed in the UK PII: S0953-8984(98)90350-2

Structure of iron niobophosphate glasses investigated by DTA, infrared and Mössbauer spectroscopy

E F de Almeida†, J A C de Paiva†, M A B de Araújo†, E B Araújo‡, J A Eiras‡ and A S B Sombra†

† Laboratório de Óptica Não-Linear e Ciência dos Materiais (LONLCM), Departamento de Física, Universidade Federal do Ceará, Caixa Postal 6030, Fortaleza CE, Brazil

‡ Departamento de Física, Grupo de Cerâmicas Ferroelétricas, Universidade Federal de São Carlos, Caixa Postal 676, São Carlos SP, Brazil

Received 6 January 1998, in final form 5 May 1998

Abstract. Activation energies for crystallization of 50 Li_2O–40 P_2O_5–10 Nb_2O_5–x Fe_2O_3 glasses, with $x = 0$, 5 and 10 mol%, were determined by differential thermal analysis (DTA). The structure was investigated by infrared and Mössbauer spectroscopy. Samples with $x = 5$ mol% of Fe_2O_3 show larger activation energy (160.9 kJ mol^{-1}). Absorptions at P–O–P, P=O, $P–O^-$ and PO_4 units are presents in these glasses. P=O absorptions disappear at compositions with $x = 5$ and 10 mol% of Fe_2O_3, which shows absorption around 571 cm^{-1}, attributed to FeO_6 units. According to Mössbauer results high spin Fe^{3+} and Fe^{2+} at distorted octahedral sites are present in samples with $x = 5$ and 10 mol% of Fe_2O_3, thus working as a network modifier.

1. Introduction

Phosphate glasses have been studied extensively in recent years. Vitreous phosphoric anhydride (P_2O_5) does not have sufficient hydroscopic resistance to be used alone. Its structure is based on distorted tetrahedral (PO_4). One interest is in the use of P_2O_5 as a network former and the possibility of forming a vitreous matrix with, for example, alkali metals (M = Li, Na) in system M_2O–Nb_2O_5–P_2O_5 [1]. The introduction of P_2O_5 into binary alkali silicate glasses has profound effect on their structure, particularly at high concentrations [2]. Phosphates of alkali metals grouping at different degrees of complexity such as isolated PO_4^{3-} tetrahedra, two tetrahedra joined and long chains or rings of PO_4^{3-}. These materials combine to form M_3PO_4 (orthophosphate), $M_4P_2O_7$ (pyophosphate) and MPO_3 (pyrophosphate) [3]. For niobium phosphate glasses, with 2 mol% of Fe_2O_3 used as impurity, $LiNbO_3$ can be crystallized inside the glass structure to form a glass–ceramic [4]. Lithium niobate, $LiNbO_3$, is a ferroelectric material, with Curie temperature of 1210 °C, with high efficiency for second harmonic generation and widely used as an optoelectronic device as in planar wave guides [5]. In the glass system Li_2O–P_2O_5–Nb_2O_5, doped with 2 mol% of Fe_3O_3, iron ions are distributed in octahedral sites, and Fe^{3+} is predominant compared with Fe^{2+} [6]. In the present work, differential thermal analysis (DTA) was used to determine activation energy of crystallization and physical characteristics of the studied glass system. Infrared (IR) and Mössbauer spectroscopy were used to study the effect of Fe_2O_3 concentration on Li_2O–P_2O_5–Nb_2O_5–Fe_2O glasses with the aim of understanding the function of the iron in the physical properties of this system.

0953-8984/98/347511+08$19.50

2. Experimental procedure

Glasses in the Li_2O–P_2O_5–Nb_2O_5–Fe_2O system were prepared from reagent grade ammonium phosphate ($NH_4H_2PO_4$), lithium carbonate (Li_2CO_3) and niobium oxide (Nb_2O_5) with iron oxide Fe_2O_3 as an impurity, by mixing reagents in appropriate proportions and heating them in platinum crucibles in an electric furnace. To prevent excessive boiling and consequent loss of mass, the water and ammonia in $NH_4H_2PO_4$ were removed by pre-heating the mixture at 200 °C for several hours before the fusion. The mixture was subsequently melted at 1150 °C for 1 h. The melt was then poured into a stainless steel mould and pressed between two stainless steel plates. The mould and plates were pre-heated to 300 °C. The glasses prepared are (50 Li_2O–40 P_2O_5–10 Nb_2O_5):x Fe_2O_3, with $x = 0$, 5 and 10 mol%. The glassy state in the quenched samples was confirmed by x-ray diffraction (XRD) analyses at room temperature using Cu Kα radiation. The glass transition temperature (T_g), temperature of onset crystallization (T_x) and melting temperature (T_m) were determined by DTA, at heating rate of 10 °C min^{-1} using STA-409 Netzsch apparatus. The DTA measurements were performed using a platinum crucible in air and a constant sample weight of 40 mg was used for all measurements. The glass densities were determined by the Archimedes method, using distillate water as immersion liquid. The IR spectra of the glasses were investigated using KBr pellets made from a mixture of powder for each glass composition investigated. The IR spectra were measured from 1400 to 400 cm^{-1} with a Bomem MB-102 spectrometer. To determine activation energy for crystallization (E), samples were crystallized at four heating rates, ϕ (5, 10, 15 and 20 °C min^{-1}). The data were analysed using the Kissinger equation [7],

$$\ln(T_p^2/\phi) = E/RT_p + \text{constant}$$

where T_p is a temperature corresponding to the maximum of the DTA crystallization peak and R is the gas constant. The activation energy was calculated from a plot of $\ln(T_p^2/\phi)$ versus $1/T_p$.

The Mössbauer absorption spectra as obtained in standard transmission geometry, using a radioactive source of ^{57}Co in Rh matrix. Measurements were carried out at room temperature on powder samples with absorber thickness 1.9 mg of natural iron per cm^2. The spectra were evaluated using the Normos fitting program that makes use of a set of Lorentzian quadrupole doublets with fixed width and isomer shift and computes the contribution of each curve to the absorption spectra by a least squares procedure. All the isomer shifts (δ) quoted are relative to metallic iron (α-Fe). The theory of Mössbauer spectroscopy is described in the literature [8].

3. Results and discussion

3.1. DTA measurements

Several DTA measurements, at four heating rates ϕ (heating rate between 5 and 20 °C min^{-1}), were performed for (50 Li_2O–40 P_2O_5–10 Nb_2O_5)–x Fe_2O_3, with $x = 0$, 5 and 10 mol%, glasses with the aim to determine activation energy E. With the maximum crystallization T_p obtained from these DTA data and respective heating rate ϕ, figure 1 was plotted. Figure 1 shows a plot of $\ln(T_p^2/\phi)$ versus $1/T_p$, for samples with $x = 0$, 5 and 10 mol% of Fe_2O_3. The activation energy E was calculated from angular coefficients to linear fits in figure 1. Table 1 summarizes the activation energy for (50 Li_2O–40 P_2O_5–10 Nb_2O_5)–x Fe_2O_3 glasses and others physical characteristics such as density (ρ), T_g, T_x

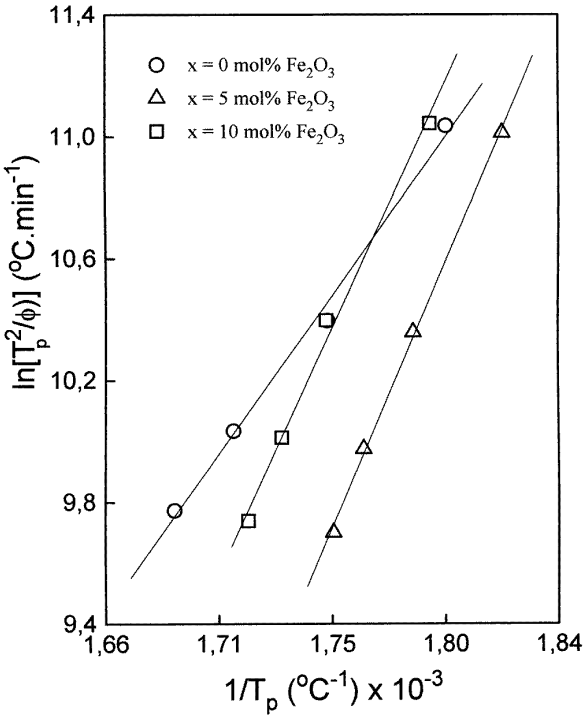

Figure 1. Plot of $\ln(T_p^2/\phi)$ versus $1/T_p$ of the 50 Li_2O–10 P_2O_5–10 Nb_2O_5–x Fe_2O_3 glasses for determination of activation energy. Points are experimental data and line are fitting at $x = 0$ mol% (○), $x = 5$ mol% (△) and $x = 10$ mol% of Fe_2O_3 (□).

and T_m. As we can see, the results show that sample with $x = 5$ mol% of Fe_2O_3 has a maximum of activation energy ($E = 160.9$ kJ mol^{-1}). The values of E determined in the present work for lithium niobophosphate glasses (table 1) are smaller than disilicate glass (250 to 290 kJ mol^{-1}), for example, reported by others [9, 10]. Activation energy was calculated at samples as prepared because, as expected, the activation energy is practically independent of the nucleation temperature and concentration of nuclei in the glass [9]. Thus, for any nucleation temperature between glass transition (T_g) and crystallization onset (T_x) temperatures, it is expected that activation energy will be the same. Glass stability can be determined qualitatively by the difference $\Delta T = T_x - T_g$. As shown in table 1, the sample without Fe_2O_3 ($x = 0$) on the glass matrix is the most stable glass, with $\Delta T = 159\,^{\circ}$C. The introduction of Fe_2O_3 in the glass matrix Li_2O–P_2O_5–Nb_2O_5 decreases thermal stability in this glass (table 1) and increases the density from 2.60 g cm^{-3} to 3.00 g cm^{-3}.

3.2. Infrared spectroscopy (IR)

Phosphate glasses are composed of PO_4 tetrahedra, which consist of long chains or rings of PO_4 sharing corners. In this work we will use the results of Corbridge and Lowe [11] and Muller [12] to interpret the IR of the phosphate glasses. According to Muller [12], absorption of the P=O group is around 1282–1205 cm^{-1} in polymeric phosphate chains. The stretching bands of P–O$^-$ (NBO—non-bridging oxygen) are around 1150–1050 cm^{-1} and 950–900 cm^{-1}. Absorption at 800–720 cm^{-1} is due to P–O–P vibrations (BO—bridging

Table 1. Physical characteristics of the 50 Li_2O–40 P_2O_5–10 Nb_2O_5–x Fe_2O_3 glasses, obtained at a heating rate of 10 °C min^{-1}.

Glass composition	Density ρ (g cm^{-3})	Glass transition temperature T_g (°C)	Crystallization temperature T_x (°C)	Melting temperature T_m (°C)	Activation energy E (kJ mol^{-1})
$x = 0$ mol%	2.60	398	557	642	96.3
$x = 5$ mol%	2.86	433	545	729	160.9
$x = 10$ mol%	3.00	461	560	728	149.4

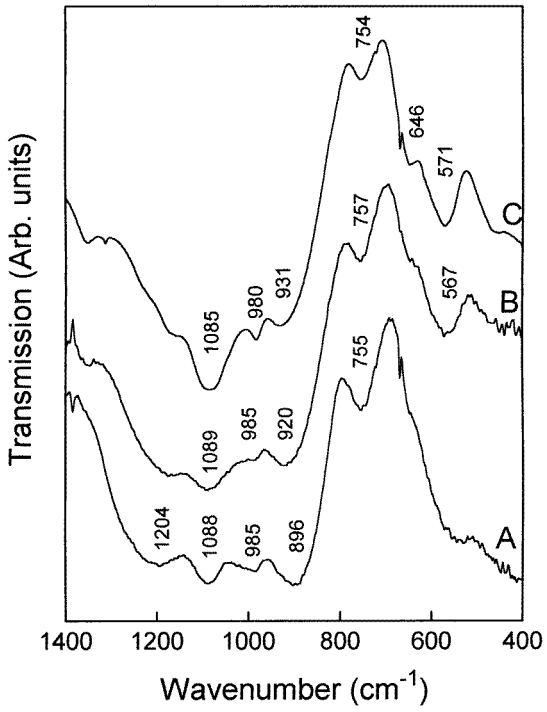

Figure 2. Infrared spectra of 50 Li_2O–40 P_2O_5–10 Nb_2O_5–x Fe_2O_3 glasses at $x = 0$ mol% (A), $x = 5$ mol% (B), and $x = 10$ mol% of Fe_2O_3 (C).

oxygen). The bands below 600 cm^{-1} are due to the bending mode of the PO_4 units in phosphate glasses.

Figure 2 shows the IR spectra of the lithium noibophosphate glasses with $x = 0$, 5 and 10 mol% of Fe_2O_3. Spectrum in figure 2(A) shows the IR spectra of the lithium niobophosphate glass without Fe_3O_3. The bands 1204 cm^{-1} (P=O), 1088 cm^{-1}, 985 cm^{-1} and 896 cm^{-1} (P–O^-), 755 cm^{-1} (P–O–P) and 543 cm^{-1} (PO_4 units) are present. With the introduction of the Fe_2O_3 in the glass matrix, in the proportion of 5 mol% and 10 mol%, figure 2(B) and (C) respectively, the resonance around 1204 cm^{-1} disappears. On the other hand, new bands around 567 cm^{-1} and 571 cm^{-1} appear (figure 2(B) and (C)).

Osaka *et al* [13] have shown that the PO_4 unit has two bridging oxygen bonds along with two non-bridging oxygen bonds as P=O and P–O^-. Therefore, the IR spectra are split into two bands with higher energy and a lower energy band. However, the iron niobophosphate

glasses studied in this work did not show splitting into these two bands. The absence of the 1204 cm^{-1} band in figure 2(B) and (C) may be associated with conversion of the P=O double bond into as bridging oxygen. The shift to higher frequency for the $P–O^-$ vibration, from 896 cm^{-1} to 931 cm^{-1} (table 2), may be due a large ionic nature of Fe–O bonds. Similar behaviour was observed by Mogus-Milankovic and Day [14] for iron phosphate glasses.

Table 2. Frequency (cm^{-1}) for IR absorptions in 50 Li_2O–40 P_2O_5–10 Nb_2O_5–x Fe_2O_3 glasses.

	Frequency (cm^{-1})		
Vibrations	$x = 0$ mol%	$x = 5$ mol%	$x = 10$ mol%
P–O–P (BO)	755	757	754
P=O	1204	NO	NO
$P–O^-$ (NBO)	1088, 985 and 896	1089, 985 and 920	1085, 980 and 931
FeO_4	NO	NO	646
FeO_6	NO	567	571

NO: not observed; NBO: non-bridging oxygen; BO: bridging oxygen.

In order to elucidate the coordination of iron for glasses studied in this work, IR spectra of Fe_2O_3 and its compounds were considered. There are two characteristic FeO_6 octahedral bands, ν_3 at 580–550 cm^{-1} and ν_4 at 470 cm^{-1}. The vibrations of FeO_4 tetrahedra are at 660–625 cm^{-1} [15]. Thus, absorption around 646 cm^{-1}, clearly present in figure 2(C), may be ascribed to the vibrations of FeO_4 tetrahedra. The presence of the absorption bands at 567 cm^{-1} and 571 cm^{-1}, figure 2(B) and (C) respectively, indicates the existence of octahedral iron FeO_6. Table 2 summarizes the absorption bands from figure 2. Abreu *et al* published very recently [16] a work studying the effect of a high level of Fe_2O_3 doping ($x \geqslant 10$ mol%) concentration in the iron niobophosphate glasses, studied by Mössbauer and infrared spectroscopy. The results show that Fe^{3+} and Fe^{2+} ions are distributed in octahedral sites and that bands around 587 cm^{-1}, 503 cm^{-1} and 480 cm^{-1} are associated with existence of octahedral iron FeO_6. The measurements also indicate that $LiFePO_4$ and α-Fe_2O_3 crystalline phases are present for high iron content samples ($x = 40$ and $x = 50$ mol%). In our present study we are concerned with the low level of doping of Fe_2O_3 ($0 \leqslant x \leqslant 10$ mol%).

3.3. Mössbauer spectroscopy

Figure 3 shows the Mössbauer spectra for samples with $x = 5$ and 10 mol% of Fe_2O_3. All the spectra in figure 3 can be interpreted as the superposition of two broad doublets. The more intense doublet can be assigned, based on isomer shift and quadrupole splitting value, to high spin Fe^{3+} (ferric iron), and the less intense to high spin Fe^{2+} (ferrous iron) [17]. We used a set of 60 Lorentzian doublets, 30 to fit the contribution to the spectrum due to Fe^{3+} and 30 for Fe^{2+}. The Lorentzian half width has been fixed at 0.12 mm s^{-1}, which is typical of a spectrum of standard metallic iron.

In table 3 are listed the Mössbauer parameters, isomer shift (δ), the most probable values of quadrupole splitting (Δ_{max}) and relative area population (A) obtained from the fit. According to Dyar [18] the Fe^{3+} ions in a octahedral coordination, present the Mössbauer parameter isomer shift (δ) with values between 0.35 and 0.55 mm s^{-1} relative to metallic iron, whereas for a tetrahedral coordination the δ value between 0.20 and 0.30 mm s^{-1}. For the Fe^{2+} ions, values of δ below 1.0 mm s^{-1} relative to metallic iron, are associated with

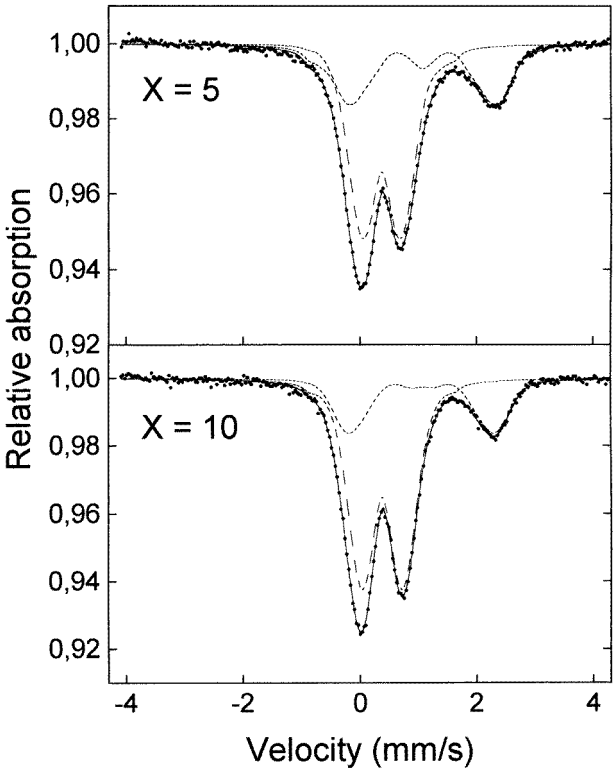

Figure 3. Mössbauer spectra of samples of $x = 5$ and $x = 10$ mol%. (●) Experimental points and the continuous line is the theoretical fitting.

Table 3. Mössbauer parameters of the 50 Li_2O–40 P_2O_5–10 Nb_2O_5–x Fe_2O_3 glasses. In this table δ (mm s^{-1}), Δ (mm s^{-1}) and A (%), are the isomer shift, quadrumpole moment and area, respectively.

	Fe^{2+}			Fe^{3+}		
Sample	δ (mm s^{-1})	Δ (mm s^{-1})	A (%)	δ (mm s^{-1})	Δ (mm s^{-1})	A (%)
$x = 5$	1.08	2.51	31	0.37	0.67	69
$x = 10$	1.05	2.50	26	0.40	0.70	74

tetrahedral coordination. The Mössbauer parameter quadrupole splitting (Δ) is also useful for evaluating the coordination number since a distorted tetrahedral site is characteristically less symmetric than a distorted octahedral site, therefore different values of Δ should be obtained. However it is observed [18] that coordination number should be primarily determined from δ values.

Recently Day *et al* [19] report results in iron phosphate glasses studied by Mössbauer spectroscopy where the valence states of iron ions in several iron phosphate glasses were studied. It was observed that the general coordination of the majority of iron ions appears to be distorted octahedral. However the Mössbauer spectra do not totally exclude the presence of some tetrahedrally coordinated iron ions in the iron phosphate glasses.

In this work, for the Fe^{3+} ion, the values of δ range from 0.37 to 0.40 mm s^{-1} and for the Fe^{2+} ion the values are between 1.08 and 1.05 mm s^{-1}, for $x = 5$ and 10 mol% of Fe_2O_3 respectively. Therefore we can assume that both ions are sites of distorted octahedral coordination, i.e. they are network modifiers. The quadrupole splitting values are also in agreement with this interpretation. Table 3 also shows the relative area population (A) for both Fe^{2+} and Fe^{3+} ions. As we can see, for both samples Fe^{3+} is predominant compared with the Fe^{2+} population.

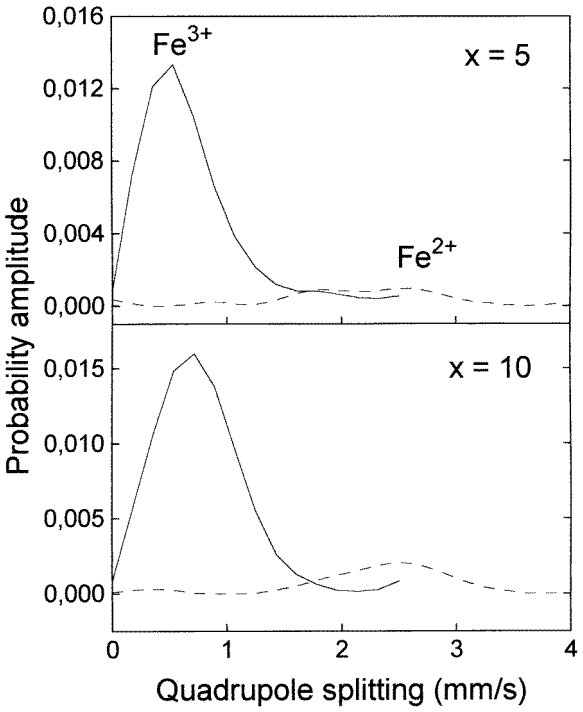

Figure 4. Quadrupole splitting distribution for Fe^{3+} and Fe^{2+} at the octahedral sites. (Samples $x = 5$ and $x = 10$ mol%.)

Figure 4 shows the probability distributions of the Lorenzian doublets versus quadrupole splitting (Δ) for Fe^{3+} and Fe^{2+} ions in samples with $x = 5$ and 10 mol% of Fe_2O_3. As we can see the distributions show different maxima of the quadrupole splitting distribution, which are associated with different distortions of the octahedral symmetry around the iron ions. The position of the Δ_{max} represents the most probable value of the quadrupole splitting of the site. For samples with $x = 5$ the Fe^{2+}, which are just 31% of the total iron, occupy two distinct sites. The site with $\Delta_{max} = 2.51$ mm s^{-1} is the one with highest probability. The Fe^{3+} in this samples (69% of the total iron) show the most probable value $\Delta_{max} = 0.67$ mm s^{-1}. For samples with $x = 10$ mol% the Fe^{2+}, which represent 26% of the total iron, occupy two distinct sites with the most probable $\Delta_{max} = 2.50$ mm s^{-1}. The Fe^{3+} (74% of the total iron) on the other hand, presents the most probable $\Delta_{max} = 0.70$ mm s^{-1}.

4. Conclusions

Iron niobophosphate glasses were investigated in the present work with DTA analysis, infrared and Mössbauer spectroscopy, to investigate the effect of the increasing concentration of Fe_2O_3 in the glass matrix. Results show that the activation energy for crystallization increases with the increase of Fe_2O_3 in the glass matrix. The sample with 5 mol% of Fe_2O_3 shows the maximum activation energy. Infrared spectra clearly indicate the presence of the P=O, P–O–P and P–O^- bands. Samples with Fe_2O_3 do not show bands associated with P=O. This absence may be associated with conversion of the P=O double bond into a bridging oxygen. High spin Fe^{2+} and Fe^{3+} (which are present in samples with $x = 5$ and 10 mol% of Fe_2O_3) are assumed to be at sites of distorted octahedral coordination (network modifier).

Acknowledgments

The authors wish to thank CNPq and FAPESP, both Brazilian agencies, for financial support. We gratefully acknowledge the Centro de Technologia da Unifor (UNIFOR) and NUTEC for use of their laboratories for sample preparation.

References

[1] El Jazouli A, Brochu R, Viala J C, Olazcuaga R, Delmas C and Le Flem G 1982 *Ann. Chim. Fr.* **7** 285–92
[2] Lewis M H (ed) 1989 *Glasses and Glass-ceramics* (London: Chapman and Hall) p 17
[3] Banishev A F, Voron'ko Yu K, Osiko V V and Sobol A A 1984 *Sov. Phys.–Dokl.* **29** 50
[4] Araújo E B, de Paiva J A C and Sombra A S B 1995 *J. Phys.: Condens. Matter* **7** 9723
[5] Abouelleil M M and Leonberger F J 1989 *J. Am. Ceram. Soc.* **72** 1311
[6] Araújo E B, de Paiva J A C, de Araújo M A B and Sombra A S B 1996 *Phys. Status Solidi* b **197** 231
[7] Kissinger H E 1956 *J. Res. Bur. Stand.* **57** 217
[8] Greenwood N N and Gibb T C 1971 *Mössbauer Spectroscopy* (London: Chapman and Hall)
[9] Hautojarvi P, Vehanen A, Kompa V and Pajane E 1978 *J. Non-Cryst. Solids* **29** 365
[10] Ray C S and Day D E 1990 *J. Am. Ceram. Soc.* **73** 439
[11] Corbridge D E C and Lowe E J 1954 *J. Chem. Soc.* **493**
[12] Muller K P 1969 *Glastechn. Ber.* **42** (3) 83
[13] Osaka A, Takahashi K and Ikdea M 1984 *J. Mater. Sci. Lett.* **3** 36
[14] Mogus-Milankovic A and Day D E 1993 *J. Non.-Cryst. Solids* **162** 275
[15] Iordanova R, Dimitriev Y, Dimitrov V and Klissurski D 1994 *J. Non-Cryst. Sol.* **167** 74
[16] de Abreu J A M, de Paiva J A C, de Figueiredo R S, de Araújo M A B and Sombra A S B 1997 *Phys. Status Solidi* a **162** 513
[17] Kurkjian C R and Sisety E A 1968 *Phys. Chem. Glasses* **9** 73
[18] Dyar M D 1986 *J. Am. Ceram. Soc.* **68** C-160
[19] Marasinghe G K, Karabulut M, Ray C S, Day D E, Shumsky M G, Yelon W B, Booth C H, Allen P G and Shuh D K 1997 *J. Non-Cryst. Solids* **222** 144